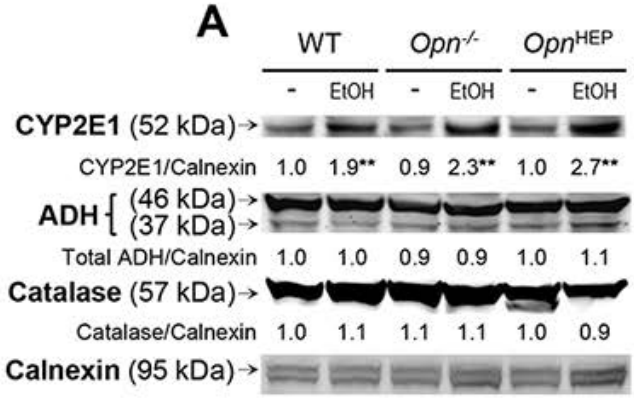

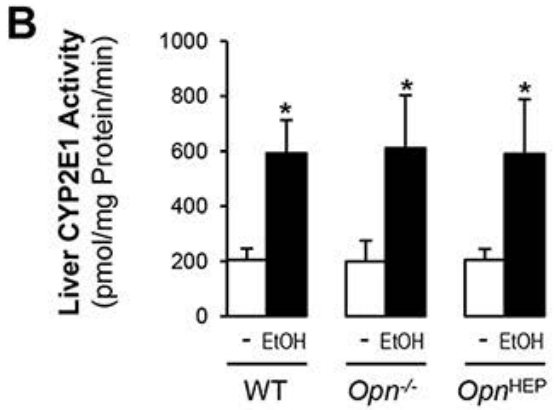

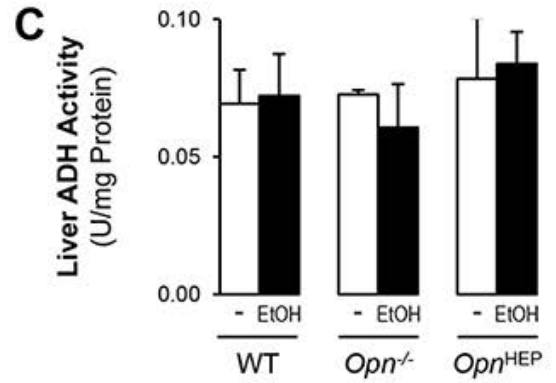

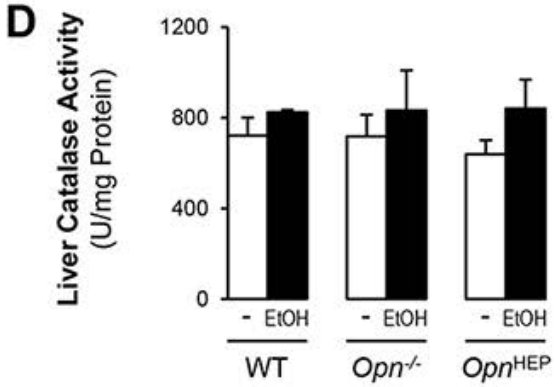

Supplementary Figure 1

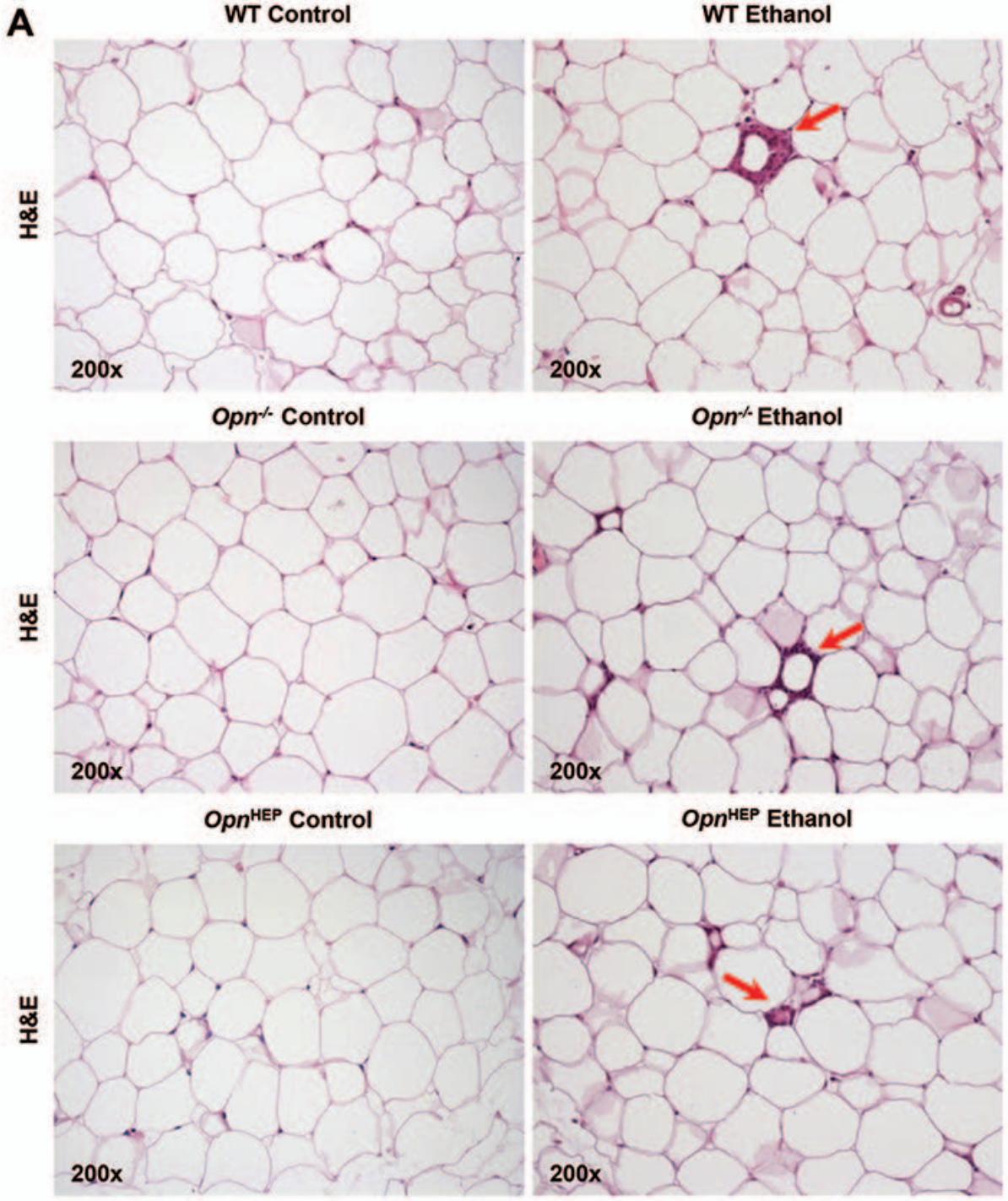

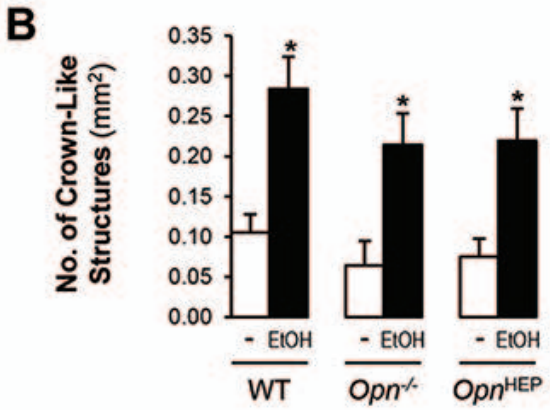

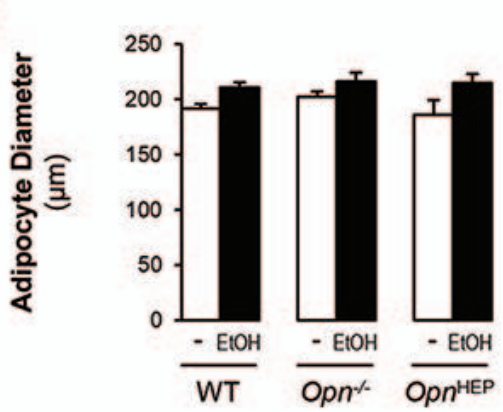

Supplementary Figure 2

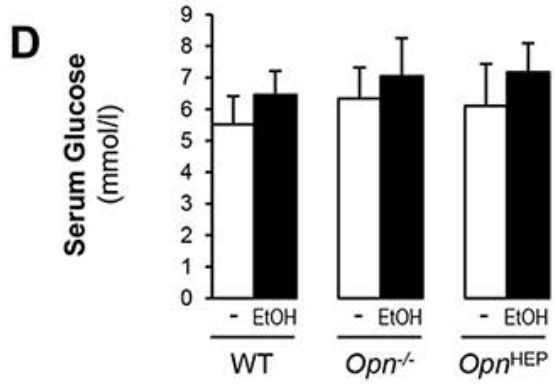

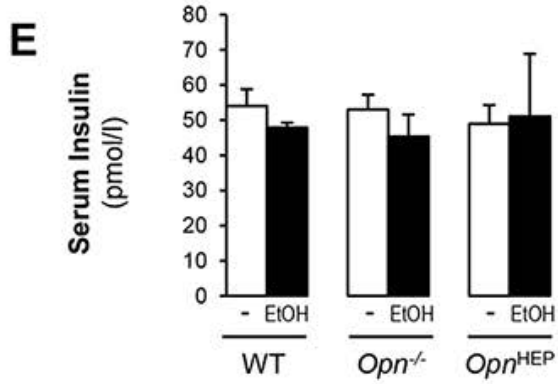

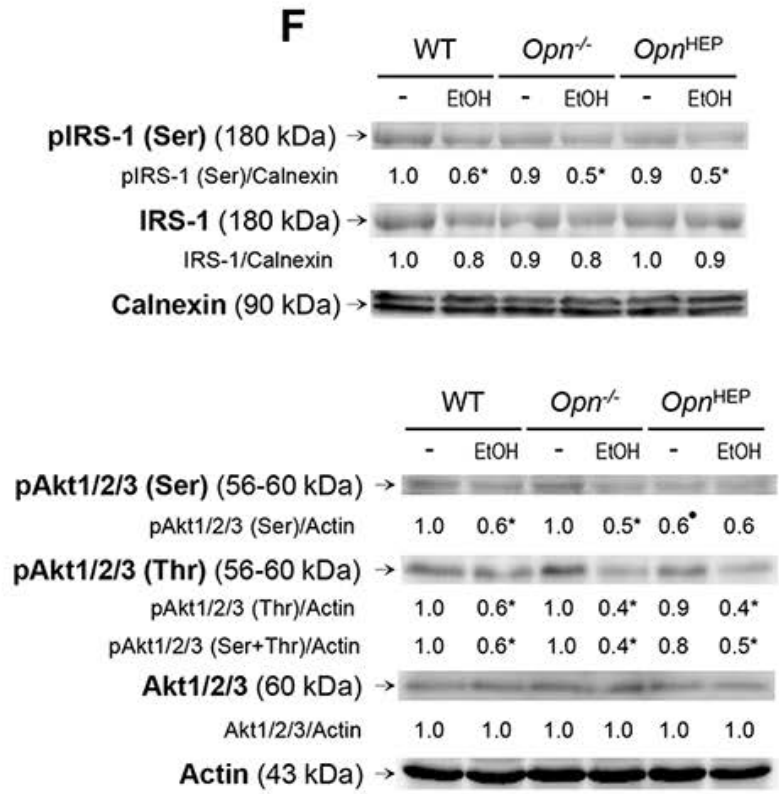

Supplementary Figure 2 Continuation

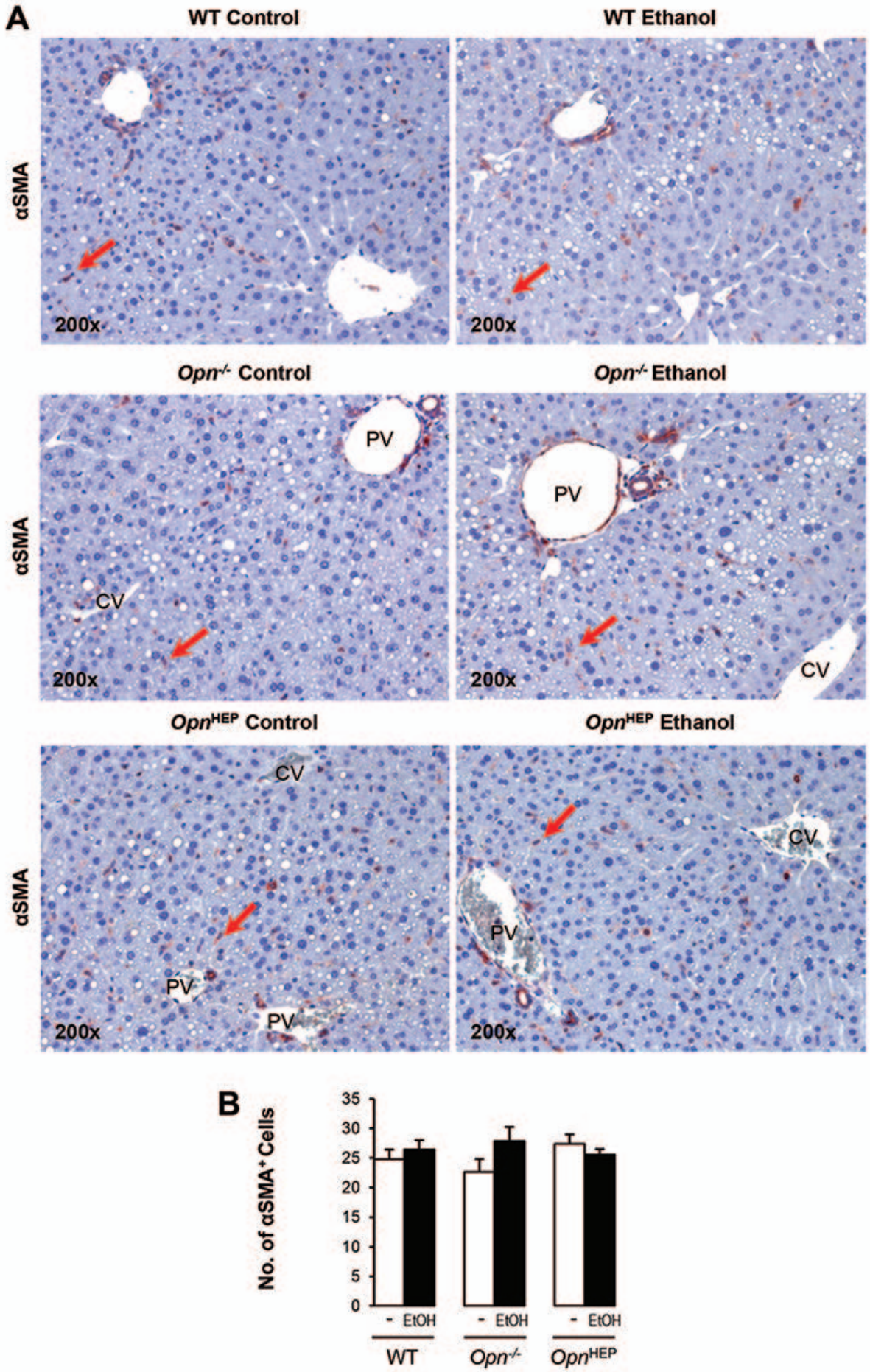

Supplementary Figure 3

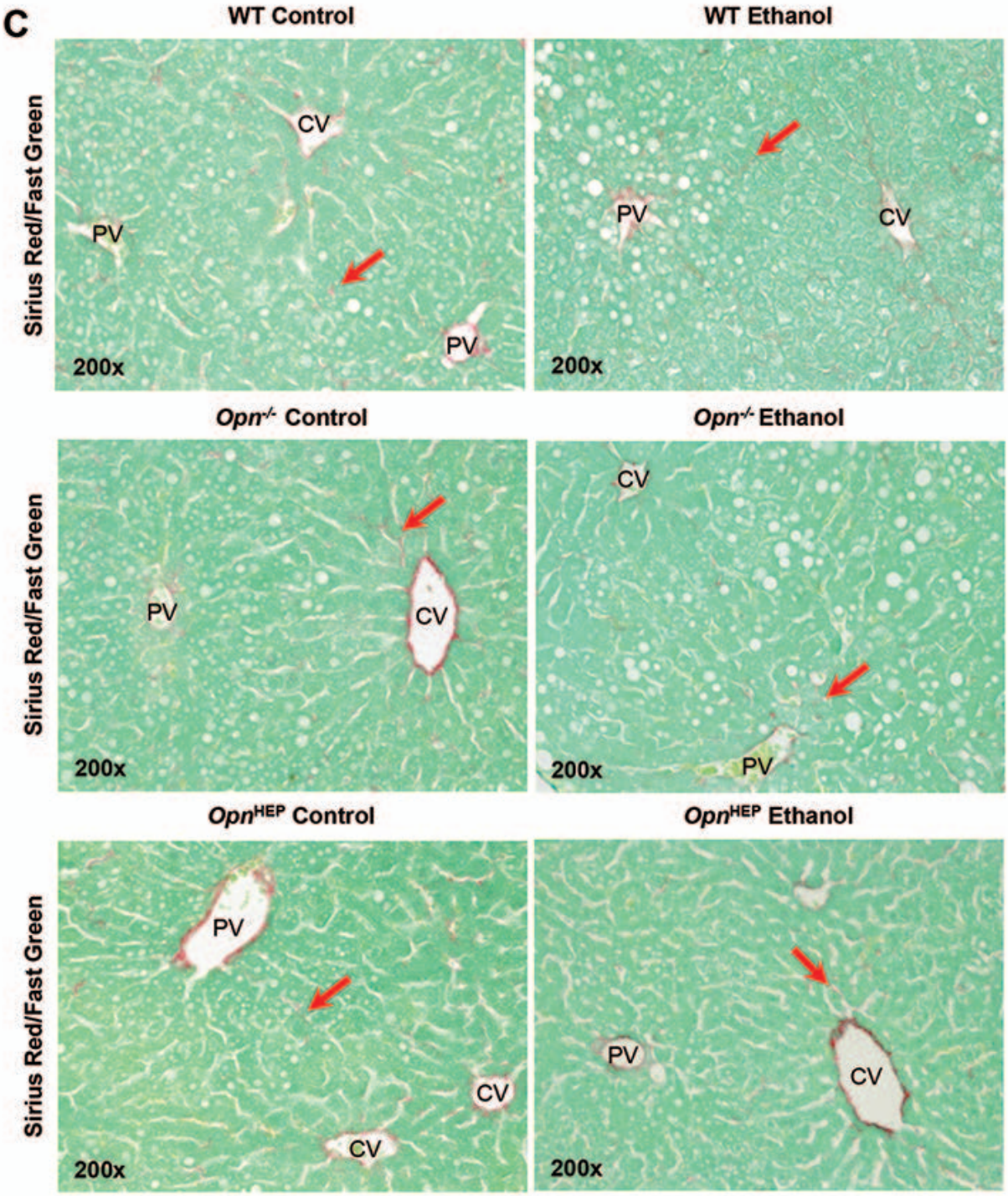

Supplementary Figure 3 Continuation

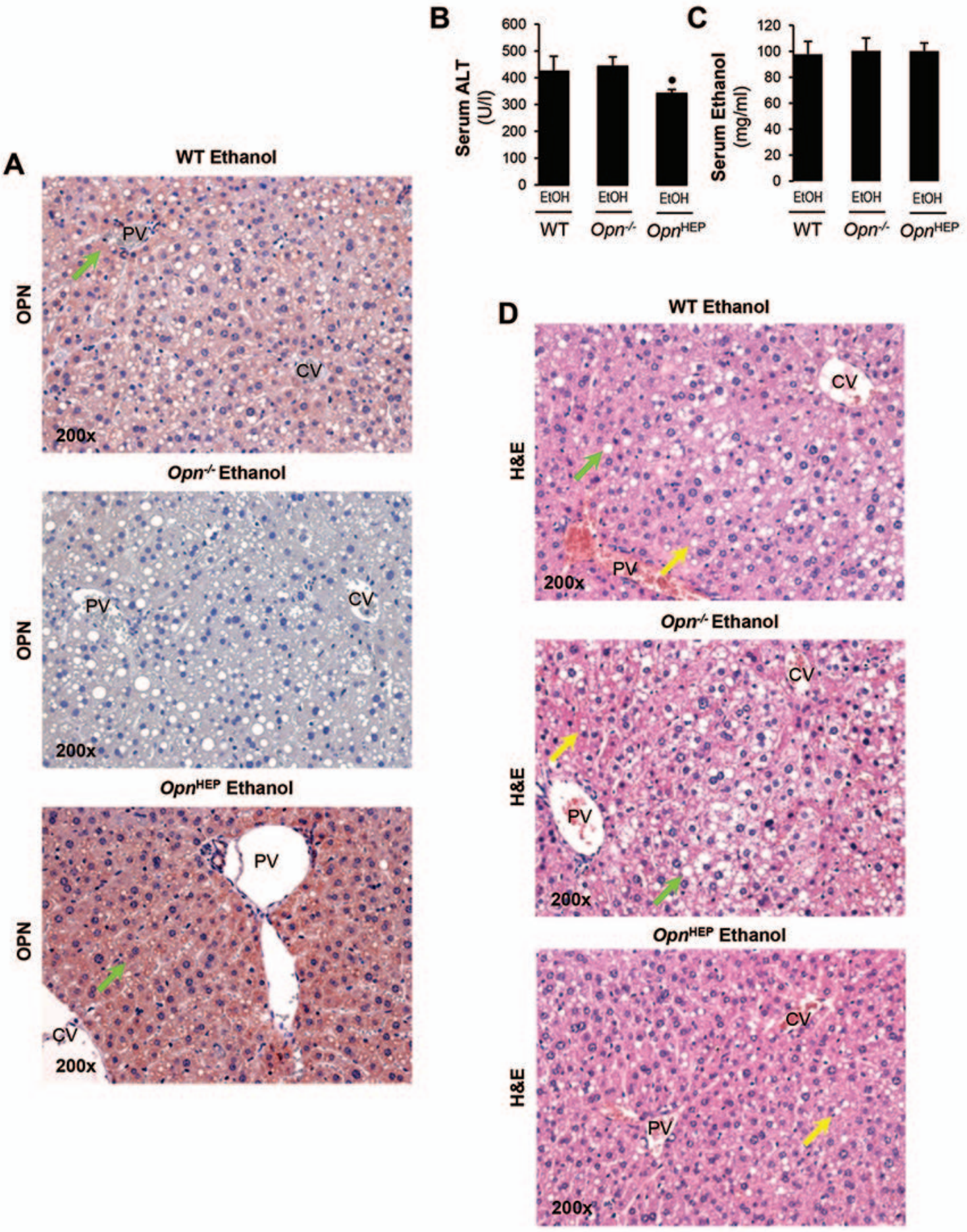

Supplementary Figure 4

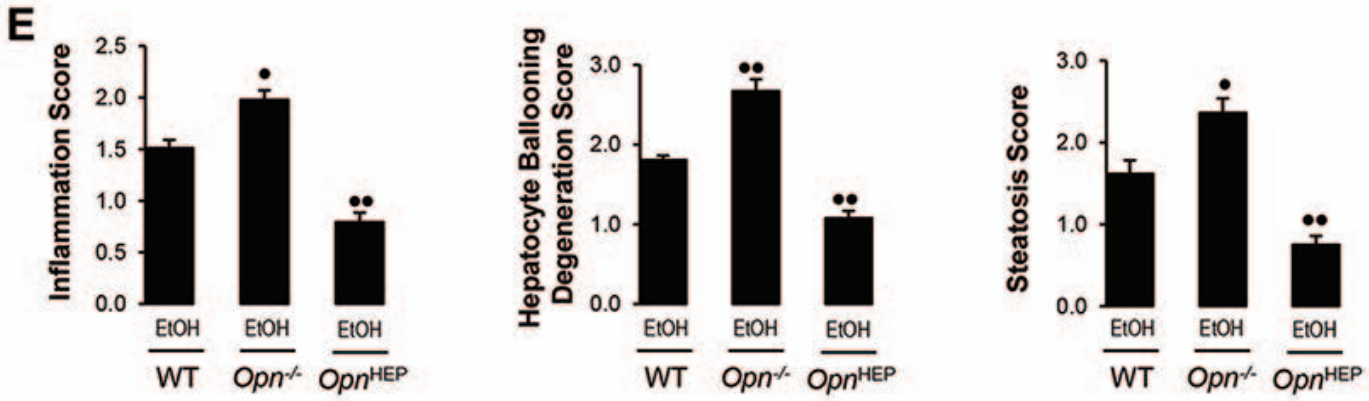

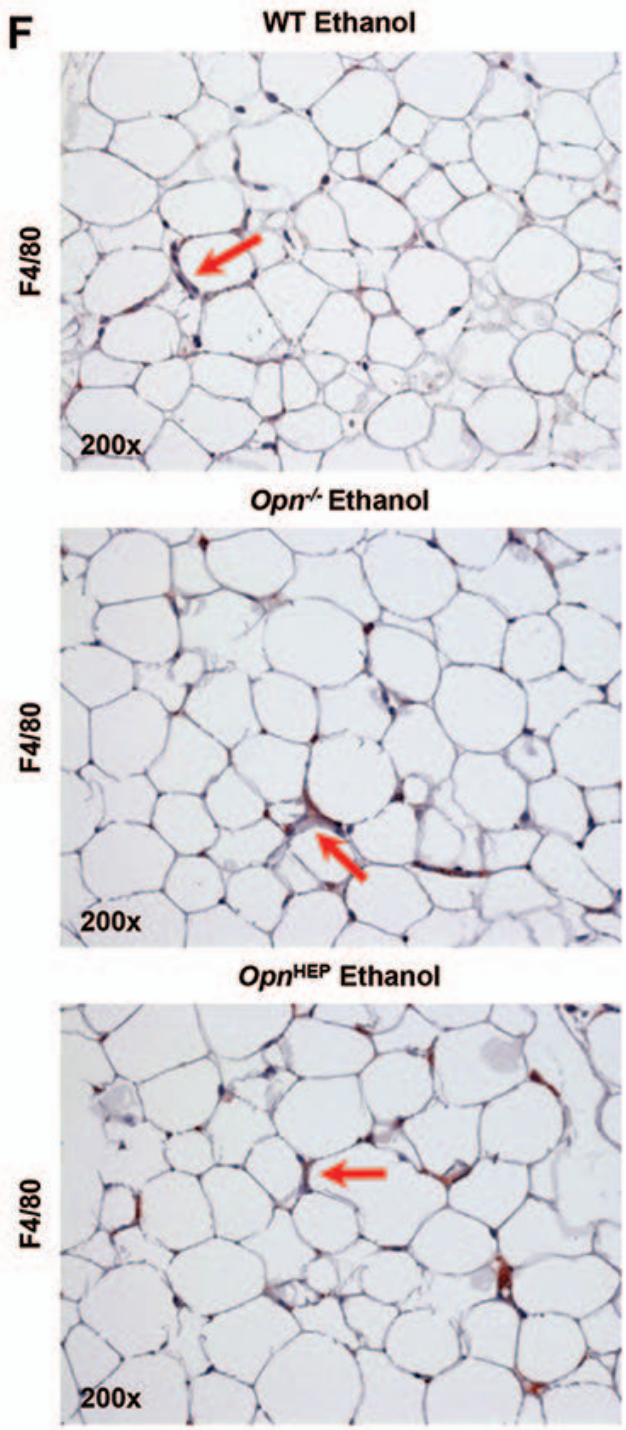

Supplementary Figure 4 Continuation

SUPPLEMENTARY MATERIAL

SUPPLEMENTARY EXPERIMENTAL PROCEDURES

General methodology. Plasma, biliary and fecal OPN was measured by ELISA (IBL, Minneapolis, MN). ALT activity, alcohol, TG and glucose were analyzed using kits (Pointe Scientific, Canton, MI). LDL and VLDL were determined with a kit (BioVision, Mountain View, CA). Insulin was measured by ELISA (Mercodia Inc, Winston Salem, NC). Total RNA extraction and qRT-PCR analysis was performed as previously (1, 2) using the following primers: *Opn* forward 5'-gagaccgtcactgctagtacaca-3', *Opn* reverse 5'-gactccttagactcaccgctctt-3', *Tnfα* forward 5'-ccagtgtgggaagctgtcct-3', *Tnfα* reverse 5'-aagcaaaagaggaggcaaca-3', *Calnexin* forward 5'-gcctgaagattgggatgaaa-3', *Calnexin* reverse 5'-caatcctctggcttctctgc-3', *16S* rRNA forward 5'-agagtttgatcctggctcag-3' and *16S* rRNA reverse 5'-tgctgcctcccgtaggagt-3'. The primers to specifically detect the most abundant Gram-negative bacteria *16S* rDNA in feces were forward 5'-ctcctacgggaggcagcag-3' and reverse 5'-gwattaccgcggckgctg-3' and were selected based on published literature (3). The following Abs were used in Western blot analysis: CYP2E1 provided by Dr. Lasker (Puracyp Inc., Carlsbad, CA), TNFα (Fitzgerald, Acton, MA), Catalase (EMD Millipore, Billerica, MA), ADH, pIRS1, IRS1, pAkt1/2/3, Akt1/2/3, Calnexin and Actin (Santa Cruz Biotechnology, Santa Cruz, CA). The 2A1 OPN Ab used in this and in our previous studies (4) was generated and donated by Dr. Denhardt (Rutgers University, NJ) (5). Ponceau red staining was performed using a kit (Sigma). The ECL reaction was developed using a Fujitsu Las4000 scanner and quantified with Image J software. ADH activity was measured according to the method of Haseba *et al* (6). Extracellular nitrites and nitrates were determined by the Griess method using a kit (Sigma). Blood and liver LPS were measured using a kit (Lonza, Walkersville, MD). Primary human Kupffer cells were isolated as previously (2). Details on general methodology such as CYP2E1 and catalase activities, Sirius red/fast green staining

as well as intra- and extracellular hydroperoxides can be found in our previous publications (4, 7-10).

Lieber-DeCarli model of early alcohol-induced liver injury. To provoke early alcohol-induced liver injury, we employed the control and the ethanol Lieber-DeCarli diets (Bio-Serv Inc., Frenchtown, NJ), which are equicaloric and have the same composition with respect to fat (42% of calories) and protein (16% of calories). Due to the presence of a high percentage of fat in these diets, steatosis, which is amplified by ethanol feeding, is expected to occur both in the control (less apparent) and in the ethanol group after a long feeding period. The content of carbohydrates is 42% of total calories (dextrin-maltose) in the control diet and 12% of total calories in the ethanol diet, where up to 30% of carbohydrate calories are replaced by ethanol (11). 10 wks old male WT, *Opn*$^{-/-}$ and *Opn*^{HEP} Tg were used in the Lieber-DeCarli model. Male mice were chosen to avoid the effect of estrogens regulating OPN expression (12). Mice were acclimatized to the liquid diet regime by feeding them the control diet for 3 d. The percentage of ethanol-derived calories was progressively increased from 10% (1 wk) to 20% (1 wk), 25% (2 wks) and 30% (3 wks). Mice were pair-fed and body weight was monitored throughout the experiment. Liver and body weight were recorded at the point of sacrifice to calculate the liver-to-body weight ratio. Blood was collected by submandibular bleeding under anesthesia and livers were removed for further analysis. All animals received humane care according to the criteria outlined in the 'Guide for the Care and Use of Laboratory Animals' prepared by the National Academy of Sciences and published by the National Institutes of Health.

Assessment of the therapeutic potential of m-OPN. To evaluate the therapeutic potential of m-OPN, 10 wks old male mice were fed the ethanol Lieber-DeCarli diets for 3 wks. This time was chosen to compare with the results from our previous publication where m-OPN was administered throughout the entire feeding period (13). The percentage of ethanol-derived

calories was progressively increased from 10% (1 wk) to 20% (1 wk) and to 30% (1 wk). Next, half of the mice received m-OPN at a concentration similar to the physiological concentration in human milk (200 µg/ml) (14, 15) dissolved in water and incorporated into the ethanol diet for 2 wks while ethanol feeding continued. Equal concentration of LPS-free BSA was used to correct for exogenous protein intake in the control group. Samples were collected as above.

The chronic-plus-single-binge ethanol feeding model of alcohol-induced liver injury. The model was performed according to (16). 10 wks old male mice were acclimatized to the control Lieber-DeCarli diet for 5 days following which they were fed ethanol for 10 days. The percentage of ethanol-derived calories was 30%. An acute administration of ethanol (5 g/kg b. wt.) was given by oral gavage the last day and mice were sacrificed 8 hours later. Samples were collected as above.

Pathology. The entire left liver lobe and the omental adipose tissue were resected and fixed in 10% neutral-buffered formalin and processed into paraffin sections for H&E staining or IHC. Blind analysis by a liver pathologist according to the Brunt classification (17) was used to determine the activity scores. Ten 100x fields per liver section from the same mouse were examined for necroinflammatory activity, which was scored as follows: 0 for none, 1 for <2 foci per 100x field, 2 for 2-4 foci per 100x field, 3 for 5-10 foci per 100x field and 4 for >10 foci per 100x field. The density of the necroinflammatory activity was also calculated per mm^2 per 100x fields. Ballooning degeneration was identified when hepatocytes were enlarged in most cases to more than twice the size of its neighboring cells. In addition, the cytoplasmic membrane became rounded instead of the usual hexagonal shape of normal hepatocytes. Most of the cytoplasm appeared empty except for a few irregular wisps of pink material representing damaged cytoplasmic content. Livers were also embedded in OCT compound, sectioned at 5 µM and stained with oil red O using standard procedures followed by morphometric assessment. Image-

Pro plus 7.0 Software (Media Cybernetics, Bethesda, MD) was used to measure the adipocyte diameter.

Immunohistochemistry. The 2A1 OPN Ab was donated by Dr. Denhardt (Rutgers University, NJ) (5). The Ab was also tested in livers from *Opn*$^{-/-}$ mice in C57BL/6J or in 129sv genetic background to ensure specificity (4). The Abs for 4-hydroxynonenal, F4/80 and TNFα were from Abcam (Cambridge, MA), EMD Millipore and Fitzgerald, respectively. The Ab for αSMA was from Sigma. Immunochemical reactions were developed using the Histostain Plus detection system (Invitrogen, Carlsbad, CA). For the computer-assisted morphometric assessment, the integrated optical density (IOD) was calculated in 10 random fields per section containing similar size portal tract or central vein at 100x and using Image-Pro plus 7.0 Software (Media Cybernetics, Bethesda, MD). The results were averaged and expressed as fold-change over the controls. The TNFα, F4/80 and αSMA indexes were calculated by counting the number of positively stained cells per field in 20 fields per slide at 200x magnification. In the adipose tissue, crown-like structures were determined by the presence of aggregates of single or fused macrophages (F4/80^{+} cells).

Source of OPN. rOPN was obtained from R&D Systems (Minneapolis, MN). M-OPN was purified from human milk or from bovine milk by anion-exchange chromatography as described elsewhere (18) (US Patent 7,259,243). The m-OPN used in our experiments is more than 97% pure OPN as analyzed by Edman sequencing, RP-HPLC and MS analysis. Bovine m-OPN has been thoroughly characterized with respect to post-translational modifications and the fragmentation pattern (19). The preparation used in the current study is glycosylated and phosphorylated. It contains 28 phosphorylation sites, which are phosphorylated by 90-100%. Likewise, the five *O*-glycosylation sites are fully occupied (19). The form of bovine m-OPN used is significantly processed by the endogenous milk protease plasmin. A significant part of the

OPN is present as the *N*-terminal fragment representing residues 1-145/147, which is in accordance with the way OPN is found in milk.

Flow cytometry. RAW 264.7 cells (mouse leukemic monocyte macrophages, $3x10^5$ cells) were incubated with 200 ng/ml FITC-LPS and 0-0.2 μM rOPN in 1 ml of DMEM-F12 for 30 min at room temperature. In some experiments TLR4 and MD2 neutralizing Abs (Santa Cruz Biotechnology, Santa Cruz, CA) were used. Cells were washed twice with DMEM-F12 and analyzed using a FACScan flow cytometer (Becton Dickinson, Franklin Lakes, NJ) and the side scatter parameter to gate the signal.

Statistical analysis. Data were analyzed by a two-factor analysis of variance and results were expressed as mean ± standard error of the mean (*n*=10/group for the *in vivo* experiments and at least *n*=6 for the *in vitro* experiments).

SUPPLEMENTARY RESULTS

The alcohol metabolizing enzymes are similar in the livers from ethanol-treated mice. Since alcohol levels were comparable in all ethanol-treated mice, we evaluated whether similar ethanol metabolism occurred as well. This was confirmed evaluating both protein expression and activity of CYP2E1 **(Supplementary Fig. 1A-1B)**, ADH **(Supplementary Fig. 1A** and **1C)** and catalase **(Supplementary Fig. 1A** and **1D)**, the liver alcohol metabolizing enzymes. All ethanol-treated mice displayed comparable CYP2E1, ADH and catalase expression and enzymatic activity henceforth attesting for similar ethanol metabolism.

Alcohol-induced lipid peroxidation remains basal in* Opn^{HEP} Tg *mice but increases in WT and* Opn$^{-/-}$ *mice. Because of the significant role of lipid peroxidation-end products in the development of ALD (20), we performed IHC to evaluate for 4-hydroxynonenal, an α,β-unsaturated hydroxylalkenal produced by lipid peroxidation in many cells. IHC and morphometric analysis showed greater 4-hydroxynonenal staining in ethanol-treated WT and *Opn*$^{-/-}$ compared to *Opn*^{HEP} Tg mice (not shown); hence, natural induction plus overexpression of OPN in hepatocytes decreases lipid peroxidation preventing alcohol hepatotoxicity.

Alcohol-induced insulin resistance is similar in all ethanol-fed mice. Because of the close association between alcohol consumption and insulin resistance in the development of liver injury, we performed H&E staining in the adipose tissue from the alcohol-fed mice **(Supplementary Fig. 2A)**. The number of crown-like structures **(Supplementary Fig. 2B)** and the average adipocyte diameter **(Supplementary Fig. 2C)** were similar in all mice fed alcohol and serum glucose and insulin remained unchanged **(Supplementary Fig. 2D-2E)**. Moreover, hepatic insulin signaling determined by measuring IRS1 and Akt phosphorylation was similar in

all ethanol-fed mice **(Supplementary Fig. 2F)**. Thus, the differences in liver injury in ethanol-treated WT, *Opn*$^{-/-}$ and *Opn*^{HEP} Tg mice are not due to changes in insulin resistance.

αSMA and Sirius red/Fast green staining are similar in the ethanol-treated mice. To determine whether differences in hepatic stellate cell activation occurred under ethanol feeding, we performed IHC and morphometry analysis for αSMA, a marker of hepatic stellate cell activation **(Supplementary Fig. 3A-3B)**, and Sirius red/Fast green staining for collagenous proteins **(Supplementary Fig. 3C)**. Both markers remained quite similar in all ethanol-fed mice.

A mouse model of chronic plus binge ethanol feeding (the NIAAA model) also shows that natural induction plus forced overexpression of OPN in hepatocytes protects from alcohol-induced liver injury and steatosis whereas natural induction of OPN does not suffice to confer full protection. In addition to the Lieber-DeCarli model of chronic alcohol feeding, we also used a second model of alcoholic liver injury due to chronic ethanol feeding plus a single ethanol binge. This protocol has been recently described to synergistically induce liver injury, inflammation and fatty liver in addition to mimic acute-on-chronic alcoholic liver injury in patients (16). Analysis by IHC showed enhanced OPN^{+} staining in ethanol-fed *Opn*^{HEP} Tg compared to WT mice **(Supplementary Fig. 4A)**. Serum ALT activity was lower in ethanol-treated *Opn*^{HEP} Tg mice but it was elevated in WT and in *Opn*$^{-/-}$ mice **(Supplementary Fig. 4B)**. All groups of ethanol-treated mice showed comparable serum ethanol concentration **(Supplementary Fig. 4C)**. H&E staining **(Supplementary Fig. 4D)** and the activity scores **(Supplementary Fig. 4E)** revealed significant protection from alcohol-induced liver injury in *Opn*^{HEP} Tg compared to WT followed by *Opn*$^{-/-}$ mice. Last, H&E (not shown) and F4/80 IHC from adipose tissue also demonstrated similar number of crown-like structures and adipocyte diameter in all the ethanol-fed mice **(Supplementary Fig. 4F)**.

SUPPLEMENTARY REFERENCES

1. Nieto N. Oxidative-stress and IL-6 mediate the fibrogenic effects of [corrected] Kupffer cells on stellate cells. Hepatology 2006;44:1487-1501.

2. Cubero FJ, Nieto N. Arachidonic acid stimulates TNFalpha production in Kupffer cells via a reactive oxygen species-pERK1/2-Egr1-dependent mechanism. Am J Physiol Gastrointest Liver Physiol 2012;303:G228-239.

3. Weisburg WG, Barns SM, Pelletier DA, Lane DJ. 16S ribosomal DNA amplification for phylogenetic study. J Bacteriol 1991;173:697-703.

4. Urtasun R, Lopategi A, George J, Leung TM, Lu Y, Wang X, Ge X, et al. Osteopontin, an oxidant stress sensitive cytokine, up-regulates collagen-I via integrin alpha(V)beta(3) engagement and PI3K/pAkt/NFkappaB signaling. Hepatology 2012;55:594-608.

5. Kazanecki CC, Kowalski AJ, Ding T, Rittling SR, Denhardt DT. Characterization of anti-osteopontin monoclonal antibodies: Binding sensitivity to post-translational modifications. J Cell Biochem 2007;102:925-935.

6. Haseba T, Kameyama K, Mashimo K, Ohno Y. Dose-Dependent Change in Elimination Kinetics of Ethanol due to Shift of Dominant Metabolizing Enzyme from ADH 1 (Class I) to ADH 3 (Class III) in Mouse. Int J Hepatol 2012;2012:408190.

7. Nieto N, Friedman SL, Cederbaum AI. Cytochrome P450 2E1-derived reactive oxygen species mediate paracrine stimulation of collagen I protein synthesis by hepatic stellate cells. J Biol Chem 2002;277:9853-9864.

8. Nieto N, Cederbaum AI. Increased Sp1-dependent transactivation of the LAMgamma 1 promoter in hepatic stellate cells co-cultured with HepG2 cells overexpressing cytochrome P450 2E1. J Biol Chem 2003;278:15360-15372.

9. Cubero FJ, Nieto N. Ethanol and arachidonic acid synergize to activate Kupffer cells and modulate the fibrogenic response via tumor necrosis factor alpha, reduced glutathione, and transforming growth factor beta-dependent mechanisms. Hepatology 2008;48:2027-2039.

10. Mormone E, Lu Y, Ge X, Fiel MI, Nieto N. Fibromodulin, an oxidative stress-sensitive proteoglycan, regulates the fibrogenic response to liver injury in mice. Gastroenterology 2012;142:612-621 e615.

11. Lieber CS, DeCarli LM. The feeding of alcohol in liquid diets: two decades of applications and 1982 update. Alcohol Clin Exp Res 1982;6:523-531.

12. Banerjee A, Rose R, Johnson GA, Burghardt RC, Ramaiah SK. The influence of estrogen on hepatobiliary osteopontin (SPP1) expression in a female rodent model of alcoholic steatohepatitis. Toxicol Pathol 2009;37:492-501.

13. Ge X, Lu Y, Leung TM, Sorensen ES, Nieto N. Milk osteopontin, a nutritional approach to prevent alcohol-induced liver injury. Am J Physiol Gastrointest Liver Physiol 2013;304:G929-939.

14. Schack L, Lange A, Kelsen J, Agnholt J, Christensen B, Petersen TE, Sorensen ES. Considerable variation in the concentration of osteopontin in human milk, bovine milk, and infant formulas. J Dairy Sci 2009;92:5378-5385.

15. da Silva AP, Ellen RP, Sorensen ES, Goldberg HA, Zohar R, Sodek J. Osteopontin attenuation of dextran sulfate sodium-induced colitis in mice. Lab Invest 2009;89:1169-1181.

16. Bertola A, Mathews S, Ki SH, Wang H, Gao B. Mouse model of chronic and binge ethanol feeding (the NIAAA model). Nat Protoc 2013;8:627-637.

17. Hubscher SG. Histological assessment of non-alcoholic fatty liver disease. Histopathology 2006;49:450-465.

18. Sorensen ES, Petersen TE. Purification and characterization of three proteins isolated from the proteose peptone fraction of bovine milk. J Dairy Res 1993;60:189-197.

19. Sorensen ES, Hojrup P, Petersen TE. Posttranslational modifications of bovine osteopontin: identification of twenty-eight phosphorylation and three O-glycosylation sites. Protein Sci 1995;4:2040-2049.

20. Smathers RL, Galligan JJ, Stewart BJ, Petersen DR. Overview of lipid peroxidation products and hepatic protein modification in alcoholic liver disease. Chem Biol Interact 2011;192:107-112.

SUPPLEMENTARY LEGEND TO FIGURES

Supplementary Figure 1. ***Analysis of CYP2E1, ADH and catalase in livers from control and ethanol-treated WT,*** **Opn**$^{-/-}$ ***and*** **Opn**^{HEP} ***Tg mice.*** Western blot analysis **(A)** along with enzymatic activities of hepatic CYP2E1 **(B)**, ADH **(C)** and catalase **(D)**. The quantification of the intensity of the signal for each protein corrected by calnexin is indicated under the blots. *n*=10/group; ***p*<0.01 for ethanol *vs* control.

Supplementary Figure 2. ***Changes in insulin resistance does not account for the differences in ethanol-induced liver injury in WT,*** **Opn**$^{-/-}$ ***and*** **Opn**^{HEP} ***Tg mice.*** WT, *Opn*$^{-/-}$ and *Opn*^{HEP} Tg mice were fed 7 wks either the control or the alcohol Lieber-DeCarli diet. H&E staining from adipose tissue **(A)**. The number of crown-like structures in the adipose tissue is similar in all the ethanol-treated mice **(B)**. Computer-assisted morphometric analysis showing similar adipocyte diameter in all the ethanol-treated mice **(C)**. Serum glucose **(D)** and insulin **(E)** levels. Western blot analysis of pIRS1 and pAkt1/2/3. The quantification of the intensity of the signal for each protein corrected by the non-phosphorylated isoform and by calnexin is indicated under the blots **(F)**. *n*=10/group; **p*<0.05 for ethanol *vs* control and ·*p*<0.05 for *Opn*^{HEP} Tg vs WT.

Supplementary Figure 3. ***αSMA expression and Sirius red/Fast green staining remains similar in all ethanol-fed mice.*** WT, *Opn*$^{-/-}$ and *Opn*^{HEP} Tg mice were fed 7 wks either the control or the alcohol Lieber-DeCarli diet. IHC depicts a similar number of αSMA^{+} cells (red arrows) in all ethanol-treated mice **(A)**. Computer-assisted morphometric analysis of the αSMA IHC calculated as the number of αSMA^{+} cells in 20 fields at 200x magnification **(B)**. Sirius red/Fast green staining for collagenous proteins (red arrows) shows no major difference among groups **(C)**. *n*=10/group.

Supplementary Figure 4. ***A mouse chronic-plus-single-binge ethanol feeding model also shows that natural induction plus forced overexpression of OPN in hepatocytes protects from alcohol-induced liver injury and steatosis whereas natural induction of OPN does not suffice to confer full protection.*** 10 wks old male mice were fed ethanol according to the chronic-plus-single-binge ethanol feeding model (16). IHC shows increased OPN staining (green arrows) by ethanol feeding in WT and more in *Opn*^{HEP} Tg mice **(A)**. Serum ALT activity **(B)** and ethanol **(C)**. H&E staining shows less inflammation, hepatocyte ballooning degeneration, micro- (yellow arrows) and macrovesicular (green arrows) steatosis in ethanol-treated *Opn*^{HEP} Tg followed by WT and by *Opn*$^{-/-}$ mice. PV: portal vein. CV: central vein **(D)**. The scores for inflammation, hepatocyte ballooning degeneration and steatosis are lower in ethanol-treated *Opn*^{HEP} Tg followed by WT and *Opn*$^{-/-}$ mice **(E)**. F4/80 IHC in adipose tissue showing similar crown-like structures (red arrows) and average adipocyte diameter in all ethanol-fed mice **(F)**. n=10/group; $\cdot p<0.05$ and $\cdot\cdot p<0.01$ for any genotype *vs* WT mice.

Supplementary Table 1. ***F4/80^{+}TNFα^{+} cells in mouse liver***

	Control	EtOH
WT	0.126 ± 0.025	0.252 ± 0.024*
Opn$^{-/-}$	0.220 ± 0.032•	0.358 ± 0.052*•
Opn^{HEP} Tg	0.123 ± 0.015	0.153 ± 0.028•

**p*<0.05 for ethanol *vs* control
•*p*<0.05 for *Opn*$^{-/-}$ and *Opn*^{HEP} Tg *vs* WT mice